Research Square

Preprints are preliminary reports that have not undergone peer review.
They should not be considered conclusive, used to inform clinical practice,
or referenced by the media as validated information.

Integrated metabolomic and transcriptomic analyses reveal the regulatory mechanisms underlying ratoon bud germination in rice varieties with different node-position dominance types

Panpan Gai
Hunan Agricultural University
Yi Liang
Hunan Agricultural University
Lian Zeng
Hunan Agricultural University
Junjie Huang
Hunan Agricultural University
Qiyuan Tang
Hunan Agricultural University
Desheng Yang
15974151291@163.com

Hunan Agricultural University

Research Article

Keywords: Yield contribution rate, Ratoon bud/tiller, Different node-position dominance types, Stubble height, Metabolome, Transcriptome

Posted Date: November 13th, 2026

DOI: https://doi.org/10.21203/rs.3.rs-11438786/v1

License: This work is licensed under a Creative Commons Attribution 4.0 International License.
Read Full License

Additional Declarations: No competing interests reported.

Integrated metabolomic and transcriptomic analyses reveal the regulatory mechanisms underlying ratoon bud germination in rice varieties with different node-position dominance types

Panpan Gai, Yi Liang[a], Lian Zeng, Junjie Huang, Qiyuan Tang * , Desheng Yang *

College of Agronomy, Hunan Agricultural University, Changsha, Hunan 410128,China

*Corresponding author

E-mail: qytang@hunau.edu.cn (Q. Tang), 15974151291@163.com (D. Yang).

Abstract: To elucidate the molecular mechanisms underlying ratoon bud germination in rice varieties with contrasting node-position dominance types, the high-node-position-dominant variety Longjingyou 1212 (LJY1212) and the low-node-position-dominant variety Yongyou 4949 (YY4949) were used as experimental materials, and transcriptomic, metabolomic, and integrated analyses were performed under stubble heights of 15 and 40 cm. The results showed that at both 15 and 40 cm stubble heights, the upper-node yield contribution rate, the number of viable buds per unit area, and the single-bud length of LJY1212 were significantly higher than those at the basal nodes, whereas YY4949 exhibited the highest values at the sub-upper nodes. Transcriptomic and metabolomic analyses showed that the germinated stem buds (N) and non-germinated stem buds (NR) of LJY1212 and YY4949 were clearly separated by PCA, whereas the separation among different stubble heights within the same variety was not distinct. Metabolomic analysis revealed that the DAMs specific to LJY1212 were enriched in central carbon metabolism and photosynthetic/carbon-fixation energy-producing pathways, while the specific metabolites of YY4949 were enriched in antioxidant and specific secondary metabolic pathways. Transcriptomic analysis showed that the DEGs specific to LJY1212 were significantly enriched in photosynthesis and glycolysis/gluconeogenesis pathways, whereas the DEGs specific to YY4949 were significantly enriched in amino acid metabolism, antioxidant, and secondary metabolism pathways. Meanwhile, zeatin biosynthesis, starch and sucrose metabolism, and ascorbate and aldarate metabolism pathways were significantly enriched in both the metabolome and transcriptome, indicating that these pathways may synergistically participate in the ratoon bud germination process. In addition, the zeatin riboside (ZR) content, sucrose content, and sucrose synthase (SS) activity in N were significantly higher than those in NR. This study systematically revealed the metabolic and transcriptional response characteristics associated with ratoon bud germination in rice varieties with contrasting node-position dominance types, providing theoretical support for research on the molecular interaction mechanisms of ratoon bud germination.

Keywords: Yield contribution rate · Ratoon bud/tiller · Different node-position dominance types · Stubble height · Metabolome · Transcriptome

1. Introduction

It is estimated that rice production will need to increase by 30% by 2050 to meet the growing demand of the population[1]. However, rice yield has approached approximately 80% of its potential genetic yield, making short-term improvement in unit yield difficult, and the continuous reduction

of arable land resources in China has limited the expansion of sown area[2,3]. In this context, increasing the annual total rice production by raising the multiple cropping index or harvest frequency has become a feasible strategic choice [4]. In recent years, however, with rising labor costs and intensifying resource input pressures, the traditional double-season rice model has faced new challenges, and exploring efficient cropping systems has become an important direction for rice production development [3].

Ratoon rice utilizes the axillary buds on the rice stubble that germinate and grow after the harvest of the main crop to form a second-season rice crop, providing a feasible pathway to increase annual total production by raising harvest frequency [5]. The annual total production of ratoon rice is comparable to that of traditional double-season rice, but labor and water inputs are reduced by 50–70%, and greenhouse gas emissions are lowered by 32–42% [6]. In addition, the costs of seeds, fertilizers, and land preparation are substantially reduced, thereby significantly improving farmers' returns [6]. Consequently, ratoon rice has attracted increasing attention.

Tillers in the ratoon season originate from dormant buds in the stem nodes of the stubble after the main crop harvest, and the developmental processes of dormant buds at different positions differ markedly [7]. Generally, ratoon buds at upper nodes germinate earlier and grow faster but have a shorter growth period, earlier heading, and smaller panicles, whereas ratoon buds at lower nodes germinate later but have a longer growth period, later heading, and larger panicles [8,9]. Based on morphological and physiological differences, cultivated rice in Asia is mainly divided into indica and japonica [10]. Furthermore, according to the germination characteristics of axillary buds, varieties can be classified into high-node-position-dominant and low-node-position-dominant types. Indica rice is mostly of the high-node-position-dominant type, with a regeneration rate of 91.97% at upper nodes (D2, D3), where axillary buds at upper nodes inhibit the germination and growth of those at lower nodes; in contrast, japonica rice is mostly of the low-node-position-dominant type, with a regeneration rate of 50.00% at lower nodes (D4), where the inhibitory effect of upper nodes is not pronounced [11]. However, systematic and in-depth investigation of the mechanisms underlying axillary bud germination in varieties with different node-position dominance types is currently lacking.

Stubble height directly determines the position and number of retained ratoon buds and regulates the growth period and ratoon tiller growth in the ratoon season [12]. Compared with low stubble, high stubble retains more ratoon buds and increases the number of panicles, but reduces the number of panicles at basal nodes, resulting in smaller panicles and a shortened growth period [13,14]. Meanwhile, apical dominance exists in ratoon bud germination, whereby upper-node ratoon buds inhibit the germination and growth of lower-node ratoon buds; the higher the stubble height, the stronger the axillary bud germination dominance, the faster the seedling emergence, and the shorter the growth period [15]. Notably, axillary buds at different nodes differ in their dependence on stem-sheath nutrients, with upper-node axillary buds showing stronger dependence due to apical dominance[16]. In addition, stubble height can regulate the growth of the ratoon root system, and

low stubble significantly promotes new root growth in the ratoon season [17]. Root function at the full-heading stage of the ratoon season is significantly linearly correlated with ratoon rice yield, and low stubble favors the occurrence of ratoon roots [14,18]. However, systematic and in-depth investigation of the mechanisms underlying axillary bud germination in varieties with different node-position dominance types under high stubble is lacking.

The nutrients required for early ratoon bud growth are supplied by the mother stubble, and non-structural carbohydrates (NSC) stored in the mother stubble are the main nutrient source promoting ratoon seedling growth. Starch in NSC is generally first converted to sucrose and then loaded and transported within the plant in the form of sucrose, providing energy and carbon skeletons for ratoon bud germination [15]. Studies have shown that the higher the soluble sugar content in each stem node before the main crop harvest, the higher the survival rate of ratoon buds [15]. In addition to serving as an energy substrate, sucrose can also act as a signaling molecule involved in regulating bud germination and branch formation [19,20]. As a signaling substance, sucrose upregulates the biosynthesis of auxin and cytokinin to indirectly promote bud growth [21]. In summary, sucrose is not only a carbon source sustaining bud growth but may also act as a signaling substance playing an initiating regulatory role in ratoon bud germination.

Plant hormones, as signaling substances in plants, play important roles in bud germination and growth. Cytokinin (CTK) is mainly synthesized in roots and transported to axillary buds via the xylem, promoting cell division and expansion [22]. In contrast, auxin (IAA) is synthesized in the apical meristem and transported basipetally through polar transport to basal tissues, thereby inhibiting lateral bud growth [23]; strigolactone (SL) is synthesized in roots and stem bases and transported upward to axillary buds, exerting inhibitory effects on bud growth in various plants [24]; abscisic acid (ABA) has been identified as a core negative regulator of bud dormancy, and its accumulation in rice nodes significantly inhibits axillary bud germination, thereby reducing ratooning ability [25]. These hormones also form a fine regulatory network through synergistic and antagonistic interactions. IAA inhibits bud germination by reducing CTK accumulation, whereas CTK promotes bud activation by counteracting IAA-mediated inhibition [26]. IAA can also act synergistically with SL signaling to enhance the inhibitory effect on ratoon bud development [27]. Meanwhile, both CTK and SL act as second messengers of IAA in regulating axillary bud germination, and the two are antagonistic. In ratoon rice, SL can inhibit CTK accumulation by accelerating the expression of CTK metabolism genes (e.g., OsCKX1, OsCKX2, and OsCKX10), thereby suppressing ratoon bud growth [28]. In summary, hormones such as IAA, CTK, and SL are interwoven through synergistic and antagonistic interactions, jointly forming a multi-hormone fine regulatory network for ratoon bud germination and growth in ratoon rice.

In recent years, the development of multi-omics technologies has provided new approaches for elucidating the regulatory mechanisms of crop growth and development. Although numerous studies have investigated the effects of different varieties and stubble heights on ratoon bud germination and yield in ratoon rice, the reasons underlying the differences in ratoon bud germination among

varieties with different node-position dominance types and under different stubble heights remain unclear, and the underlying physiological and molecular regulatory mechanisms require further elucidation. Therefore, in this study, the high-node-position-dominant variety LJY1212 and the low-node-position-dominant variety YY4949 were selected, and two stubble heights (15 cm and 40 cm) were established. By integrating physiological measurements with metabolomic and transcriptomic analyses, the regulatory mechanisms of ratooning in ratoon rice varieties with different node-position dominance types were systematically elucidated. This study aimed to address: (1) whether intrinsic differences exist in the regulatory mechanisms of ratoon bud germination between varieties with different node-position dominance types, and (2) whether ratoon bud germination under different stubble heights follows the same regulatory mechanisms.

2. Materials and Methods

2.1. Site description

The experiment was conducted from 2024 to 2025 in Qianshanhong Town, Datonghu District, Yiyang City, Hunan Province (112°43′E, 29°13′N). The ratoon rice growing season spans March to November each year, and in recent years both the experimental field and adjacent fields had ratoon rice as the previous crop. The region has a subtropical monsoon climate. Before basal fertilizer application, soil samples from the 0–20 cm tillage layer were collected to determine physicochemical properties. The soil texture is derived from fluvial-lacustrine sediments. In 2024, the soil pH was 7.59, organic matter was 48.4 g kg^{-1}, total nitrogen was 2.5%, available phosphorus was 10.2 mg kg^{-1}, and available potassium was 96.3 mg kg^{-1}; in 2025, the soil pH was 7.87, organic matter was 35.4 g kg^{-1}, total nitrogen was 2.8%, available phosphorus was 14.3 mg kg^{-1}, and available potassium was 110.9 mg kg^{-1}. Daily minimum and maximum temperature and precipitation data for the two years were downloaded from the China Meteorological Data Network (http://www.nmic.cn/).

2.2. Experimental design and crop management

A split-plot design was adopted, with variety as the main plot and stubble height treatment as the subplot. The plot area was 25 m^2 (5 m × 5 m), with three replications. The high-node-position-dominant variety Longjingyou 1212 (LJY1212) and the low-node-position-dominant variety Yongyou 4949 (YY4949) were used as experimental materials. Two stubble heights, 15 cm and 40 cm, were established. The 15 cm stubble retained nodes 3, 4, and 5 (with node 3 potentially removed by cutting), whereas the 40 cm stubble retained nodes 2, 3, 4, and 5.

Seedlings were raised in mechanical throwing trays in a greenhouse. Sowing dates were March 25, 2024 and March 22, 2025, and transplanting dates were April 19, 2024 and April 16, 2025, with a plant spacing of 20 cm × 20 cm and two seedlings per hill. A uniform fertilization scheme was applied across all experimental plots. In the main crop, 180 kg N ha^{-1}, 40 kg P ha^{-1}, and 60 kg K ha^{-1} were applied. Nitrogen fertilizer was applied at a basal:tillering:panicle ratio of 5:3:2, at 1 d before transplanting, 10 d after transplanting, and at the panicle initiation stage, respectively; phosphorus

fertilizer was applied entirely as basal fertilizer in a single application; and potassium fertilizer was applied at a basal:panicle ratio of 1:1 and mixed with nitrogen fertilizer. In the ratoon season, 75 kg N ha^{-1} was applied 15 d after full heading of the main crop as a bud-promoting fertilizer, and 100 kg N ha^{-1} was applied within 3 d after main crop harvest as a seedling-promoting fertilizer.

Water management in the main crop: a 2–3 cm water layer was maintained in the field from transplanting until 80% of the target tiller number was reached, after which the field was drained and sun-dried for approximately 2 weeks, then re-flooded to maintain a 2–3 cm water layer until 7 d before harvest; from 7 d before harvest to maturity, the field was drained and sun-dried. Water management in the ratoon season was conducted separately for high and low stubble treatments. After main crop harvest, the high-stubble plots were immediately irrigated, and a 2–3 cm water layer was maintained until 10 d before harvest; from 10 d before harvest to maturity, the field was drained and sun-dried. After main crop harvest, the low-stubble plots were irrigated with running water in the evening and drained the next morning, leaving only a shallow water layer; this operation was repeated until the low-node ratoon seedlings stabilized and reached the two-leaf-one-heart stage, after which water management was unified with that of the high-stubble treatment. To prevent water and fertilizer leakage between plots, each plot was separated by ridges with plastic film (0.8 m wide) inserted into the soil. During the experiment, weeds, diseases, and pests were strictly controlled by chemical agents.

2.3. Yield and Yield Components

At maturity of the ratoon crop (RC), 12 hills were sampled from each plot after excluding three rows from the lateral and longitudinal borders, and the samples were separated into stubble and ratoon tillers. Ratoon panicles were grouped by node position (for the 40 cm stubble, the retained nodes from top to base were designated D2, D3, D4, and D5; for the 15 cm stubble, the retained nodes from top to base were designated D3, D4, and D5), and the number of productive panicles was recorded for each group. The samples were then manually threshed and naturally air-dried, and filled and unfilled grains were separated by water flotation. After sun-drying, the grains were oven-dried for 72 h. Using an electronic balance with a precision of 0.001 g, three 30 g subsamples of filled grains and three 3 g subsamples of unfilled grains were weighed for each treatment, and the numbers of filled and unfilled grains were recorded and averaged. Finally, spikelets per panicle, seed-setting rate, and 1000-grain weight were calculated.

2.4. Ratoon bud/tiller length and number of viable buds/tillers per unit area

From 15 d after full heading of the main crop to the full heading stage of the ratoon season, two uniformly growing hills were selected from each plot every 5 d. Ratoon buds/tillers at nodes D2, D3, D4, and D5 were detached from the mother stems by node position, and the number of viable buds/tillers at each node was recorded. The length of buds/tillers at each node was measured, and the number of viable buds/tillers and bud/tiller length were calculated separately as follows:

Number of ratoon buds/tillers per unit area = number of viable buds/tillers at each node (bud

length > 1 cm) / ground area occupied by two hills of rice

Bud/tiller length (cm) = sum of bud/tiller lengths at each node / number of buds

Bud/tiller dry weight (g) = sum of bud/tiller dry weights at each node / number of buds

2.5 Transcriptomics, and metabolomics

2.5.1 Transcriptomic and Metabolomic Sampling Scheme

At 3 d after main crop harvest, two uniformly growing hills were selected from each plot and removed with roots intact, and five uniformly growing individual stems were selected from each hill. After peeling off the leaf sheaths, under the 15 cm stubble treatment, the positions where ratoon buds were attached to the stem nodes of LJY1212 D3 and D5 were designated as L15R and L15NR, respectively. Approximately 2 cm stem segments with attached ratoon buds were excised with scissors, placed separately into labeled self-sealing bags, and immediately stored in liquid nitrogen. Sampling procedures for the other treatments were the same: under the 40 cm stubble treatment, LJY1212 D3 and D5 were designated as L40R and L40NR, respectively; under the 15 cm stubble treatment, YY4949 D4 and D5 were designated as Y15R and Y15NR, respectively; and under the 40 cm stubble treatment, YY4949 D3 and D5 were designated as Y40R and Y40NR, respectively. Subsequently, the samples were transported from the experimental base back to the university and stored in an ultra-low-temperature freezer at −80°C until use. Here, R represents germinated nodes and NR represents non-germinated nodes; L and Y represent LJY1212 and YY4949, respectively; and 15 and 40 represent stubble heights. Accordingly, LR includes L15R and L40R, LNR includes L15NR and L40NR, YR includes Y15R and Y40R, and YNR includes Y15NR and Y40NR. For metabolomic analysis, six independent biological replicates were set for each treatment. For transcriptomic analysis, three independent biological replicates were set for each treatment.

2.5.2 Metabolome determination

A 100 mg sample ground in liquid nitrogen was extracted with 500 μL of 80% aqueous methanol, vortexed, incubated on ice for 5 min, and centrifuged at 15,000 × g and 4°C for 20 min. An aliquot of the supernatant was then diluted with MS-grade water to a methanol content of 53% and centrifuged at 15,000 × g and 4°C for 20 min. The supernatant was collected and injected for LC-MS analysis. QC samples were prepared by pooling equal volumes of all samples and used to equilibrate the system and monitor instrument performance; blank samples consisted of 53% aqueous methanol and were subjected to the same pretreatment as the experimental samples. Raw data were converted to mzXML format using ProteoWizard, and peak extraction, peak quantification, and peak alignment were performed using XCMS. Metabolites were identified by comparison with the NovoMetDB in-house database (Novogene) based on a 10 ppm mass deviation and adduct ion information. After normalization of the raw quantitative values, compounds with CV > 30% in QC samples were removed to obtain the metabolite identification and relative quantification results. Principal component analysis (PCA) and partial least squares discriminant analysis (PLS-DA) were performed using metaX software, and the stability of the PLS-DA model

was evaluated by permutation testing. Differentially accumulated metabolites (DAMs) were screened based on VIP ≥ 1, FC ≥ 1, and $P < 0.05$.

2.5.3 Transcriptome determination

RNA-seq was performed on the Illumina platform. Raw sequencing data were filtered using fastp to obtain high-quality clean reads, which were then aligned to the Oryza sativa L. ssp. japonica reference genome (ASM3414082v1) using HISAT2. StringTie was used for novel gene prediction, featureCounts was used to count gene reads and calculate FPKM values, and edgeR was used for differential expression analysis. Differentially expressed genes (DEGs) were screened using the criteria of $|\log_2 FoldChange| \geq 1$ and adjusted P value (padj) < 0.05. GO functional enrichment and KEGG pathway enrichment analyses were performed using clusterProfiler, with the significance threshold set at $P < 0.05$.

2.6. qRT-PCR

Four differentially expressed genes were selected for qRT-PCR validation. Total RNA was extracted from the samples using the TRIzol method, and RNA quality and concentration were assessed with a NanoDrop. cDNA was synthesized by reverse transcription using HiScript II Q RT SuperMix (Vazyme, China). Using cDNA as the template, amplification was performed on a CFX96 real-time fluorescence quantitative PCR system (Bio-Rad). The reaction system was 10 μL, including 2 μL cDNA, 5 μL 2× SYBR Green Fast qPCR Mix, 0.5 μL primers, and 2.5 μL ddH_2O. OsActin1 was used as the internal reference gene, with three replicates per sample, and the relative gene expression levels were calculated using the $2^{-\Delta\Delta Ct}$ method. The primer sequences are listed in Table S1.

2.7. Determination of zeatin riboside (ZR) and sucrose contents and sucrose synthase activity

Zeatin riboside (ZR) was extracted and purified according to the method of Bollmark et al. (1988) with modifications. Sucrose content and sucrose synthase activity were determined using commercial kits (Beijing Boxbio Science & Technology Co., Ltd., China) on a microplate reader.

2.8. Statistical data analysis

Data from each treatment with three biological replicates were subjected to analysis of variance (ANOVA) and least significant difference. Microsoft Excel was used for data collection and DPS for data analysis.GraphPad prism 9 software was used to plot the data. Metware Cloud was used to create principal component analysis (PCA) plots and cluster heat maps. PCA and Venn diagrams were generated using the Novogene Cloud Platform (https://magic-plus.novogene.com/).

3. Results

3.1 Yield and Yield Components

Under the 40 cm stubble treatment, the average ratoon-season yield of LJY1212 increased by 13.08% compared with the 15 cm stubble treatment, whereas that of YY4949 decreased by 12.21%. Under both 15 and 40 cm stubble treatments, LJY1212 exhibited the highest ratoon tiller yield at

the uppermost node, whereas YY4949 exhibited the highest yield at the sub-upper node (Fig. S1). Under the 15 cm stubble treatment, the average yield contribution rates of D3, D4, and D5 for LJY1212 and YY4949 were 54.95%, 29.00%, and 16.05%, and 15.73%, 42.07%, and 42.20%, respectively; under the 40 cm stubble treatment, the corresponding average yield contribution rates were 77.98%, 17.23%, 1.25%, and 3.55%, and 25.01%, 54.88%, 10.90%, and 9.21%, respectively (Fig. 1).

3.2 Ratoon bud/tiller length and number of viable buds/tillers per unit area

Under both 15 and 40 cm stubble heights, LJY1212 exhibited the greatest ratoon tiller length and the highest number of viable buds per unit area at the uppermost node (D3 or D2), with both parameters decreasing successively as node position moved downward, and this pattern was consistent across years (Fig. 2a, b, e, f; Fig. 3a, b, e, f). Under the 15 cm stubble treatment, YY4949 exhibited the longest ratoon tillers and the highest number of viable buds per unit area at the basal nodes (D4 and D5), with D3 significantly lower than D4 and D5; under the 40 cm stubble treatment, YY4949 exhibited the longest ratoon tillers and the highest number of viable buds per unit area at node D3, with D2 significantly lower than D3 but significantly higher than D4 and D5 (Fig. 2c, d, g, h; Fig. 3c, d, g, h).

3.3 Transcriptomic analysis

To elucidate the differences in transcriptional regulation underlying ratoon bud germination between varieties with different node-position dominance types, stem buds from germinated and non-germinated nodes of LJY1212 and YY4949 were sampled at 3 d after main crop harvest under 15 and 40 cm stubble heights for transcriptomic analysis. PCA showed clear separation between varieties, whereas separation among different stubble heights within the same variety was not distinct (Fig. 4A). Sample correlation analysis further indicated high consistency among replicates within each group (Fig. S3). A total of 10,705 and 8,912 differentially expressed genes (DEGs) were detected in LR vs. LNR and YR vs. YNR, respectively (Fig. 4B), with 5,281 DEGs shared between the two comparisons. Among these, LJY1212 had 5,944 upregulated and 4,761 downregulated DEGs, whereas YY4949 had 5,154 upregulated and 3,758 downregulated DEGs, indicating that more DEGs were detected in LJY1212 during ratoon bud germination (Fig. 4C). GO enrichment analysis showed that the DEGs shared by LJY1212 and YY4949 were mainly involved in cytoskeletal dynamic reorganization, DNA replication, and chromatin remodeling; the DEGs specific to LJY1212 were mainly involved in the regulation of protein synthesis and photosynthetic structures, whereas those specific to YY4949 were mainly involved in the regulation of antioxidant defense and redox homeostasis (Fig. 4D). KEGG enrichment analysis showed that the DEGs shared by LJY1212 and YY4949 were mainly involved in secondary metabolism, antioxidation, carbon metabolism, and hormone signal transduction; the DEGs specific to LJY1212 were mainly involved in the regulation of protein synthesis, photosynthetic energy supply, and fatty acid metabolism, whereas those specific to YY4949 were mainly involved in the regulation of sulfur-containing

amino acid metabolism, sugar metabolism, lipid metabolism, and antioxidant defense (Fig. 4E).To validate the reliability of the RNA-seq data, 12 DEGs were randomly selected for qRT-PCR analysis. The expression patterns obtained by qRT-PCR were generally consistent with those derived from RNA-seq, indicating the reliability of the transcriptomic data (Fig. S7).

3.4 Metabolomic analysis

PCA based on all differentially accumulated metabolites (DAMs) showed that QC samples and biological replicates within groups clustered tightly, whereas samples from different groups were clearly separated, indicating significant differences in metabolite accumulation patterns between the LN vs. LNR and YN vs. YNR comparisons (Fig. 5A). A total of 1,925 and 1,552 DAMs were detected in LJY1212 and YY4949, respectively, and these DAMs were assigned to 17 and 16 metabolite classes, respectively; only LJY1212 had an additional class, signaling molecules and interaction, and the two varieties shared 970 DAMs (Fig. S2 and Fig. 5B). Among these, 962 metabolites were upregulated and 963 were downregulated in LR vs. LNR, whereas 946 were upregulated and 612 were downregulated in YR vs. YNR, indicating more extensive metabolic changes during ratoon bud germination in LJY1212 (Fig. 5C). KEGG enrichment analysis showed that the metabolites shared by the two varieties were enriched in pathways such as amino acid metabolism, sugar and carbon metabolism, lipid metabolism, antioxidant metabolism, and secondary metabolism, whereas the metabolites specific to LJY1212 were enriched in central carbon metabolism, photosynthetic/carbon-fixation energy production, and plant hormone signal transduction pathways, and the DAMs specific to YY4949 were mainly enriched in hormone biosynthetic metabolism and antioxidant and specific secondary metabolic pathways (Fig. 5D and Table S1). K-means clustering analysis was used to classify the DAMs into four groups, which were enriched in secondary metabolism, plant hormone signal transduction, tryptophan metabolism, and amino acid and carbon metabolism, respectively (Fig. 5E and F).

3.5 Conjoint Transcriptomic–Metabolomic Profiling Analysis

Integrated KEGG enrichment analysis of the transcriptome and metabolome showed that zeatin biosynthesis, starch and sucrose metabolism, and ascorbate and aldarate metabolism were enriched in both omics datasets (Fig. 6). In the zeatin biosynthesis pathway, a total of 11 DEGs were detected, with 7 genes downregulated and 4 genes upregulated. The downregulated genes mainly encoded isopentenyltransferase (IPT), glucosyltransferase (CISZOG), UDP-glycosyltransferase (UGT73C), and cytokinin oxidase (CKX), whereas the upregulated genes encoded cytokinin oxidase (CKX). Meanwhile, the metabolites adenine and 5′-methylthioadenosine were upregulated (Fig. 6a).

In the starch and sucrose metabolism pathway, a total of 52 differentially expressed genes were detected. The upregulated genes mainly encoded glucosamine-6-phosphate isomerase 1/2/3 (GN1_2_3), glucosamine-6-phosphate N-acetyltransferase 5/6 (GN5_6), and β-glucosidase (bglB, bglX), whereas the downregulated genes mainly encoded trehalose-6-phosphate phosphatase (otsB) and α-amylase (AMY). Meanwhile, sucrose synthase (SUS), invertase (INV), hexokinase (HK),

starch branching enzyme (GBE1), and glucose pyrophosphorylase (glgC) each included both upregulated and downregulated members. The upregulated and downregulated genes differed between varieties. In LJY1212, trehalose-6-phosphate synthase (TPS), granule-bound starch synthase (WAXY), and phosphoglucomutase (pgm) were predominantly downregulated, sucrose phosphate synthase (SPS) included both upregulated and downregulated members, whereas starch debranching enzyme (ISA) and glycogen phosphorylase (PYG) were predominantly upregulated. In YY4949, TPS, pgm, SPS, and ISA were predominantly upregulated, whereas WAXY and PYG were predominantly downregulated. In addition, the metabolite trehalose was significantly upregulated (Fig. 6b).

In the ascorbate biosynthesis pathway, a total of 20 differentially expressed genes were detected in the ratoon bud germination groups of LJY1212 and YY4949, of which 14 were upregulated and 6 were downregulated (Fig. 6c). The downregulated genes mainly encoded L-gulonate kinase (GLCAK), whereas the upregulated genes mainly encoded L-galactose-1-phosphate phosphatase (VTC4), dehydroascorbate reductase (DHAR), L-gulonate reductase (AKR1A1), L-gulonate oxidase (GULO), and GDP-L-galactose phosphorylase (VTC5); aldehyde dehydrogenase (ALDH) and UDP-glucuronate 4-epimerase (CAF) included both upregulated and downregulated genes. Meanwhile, the metabolites L-gulose and L-threonate were upregulated, whereas the metabolite 2-oxoglutarate was downregulated (Fig. 6c).

3.6 Zeatin riboside, sucrose, and sucrose synthase activity

Under the 15 and 40 cm stubble treatments, the zeatin riboside (ZR) content, sucrose content, and sucrose synthase (SS) activity at germinated nodes (N) were 0.34- and 1.73-fold, 0.37- and 2.77-fold, and 20.75- and 6.57-fold higher, respectively, than those at non-germinated nodes (NR) in LJY1212, whereas in YY4949 they were 0.20- and 0.88-fold, 0.81- and 0.36-fold, and 13.35- and 6.03-fold higher, respectively (Fig. 7).

4. Discussion

4.1 Effects of stubble height on yield and yield contribution rate of rice varieties with different node-position dominance types

The dominant ratoon node positions, and thus the appropriate node heights, differ greatly among rice varieties, so the suitable stubble height must be determined according to the ratooning characteristics of each variety[14,29]. In this study, LJY1212 achieved high yield under the 40 cm stubble treatment, whereas YY4949 performed better under the 15 cm stubble treatment (Fig. S1). The yield of LJY1212 was mainly derived from the uppermost nodes (D3 or D2), and the yield contribution rate of the other nodes decreased as node position moved downward (Fig. 1). Under the 15 cm stubble treatment, the basal nodes (D4 and D5) of YY4949 contributed 84.27% of the ratoon-season yield; under the 40 cm stubble treatment, the yield of YY4949 was mainly derived from D3 (Fig. 1), which is broadly consistent with the findings of [30]. Studies have shown that the ratoon-season yield of high-node-position-dominant varieties is mainly contributed by the second-

and third-uppermost nodes, with a contribution rate exceeding 70%, whereas that of low-node-position-dominant varieties is mainly contributed by basal nodes, with a contribution rate exceeding 75.0% [31].

4.2 Effects of stubble height on ratoon tiller and ratoon root growth in rice varieties with different node-position dominance types

Ratoon rice axillary buds are divided into upper buds (the second- and third-uppermost nodes) and lower buds (the fourth- to sixth-uppermost nodes). Generally, indica rice has stronger germination ability at upper nodes, whereas japonica rice mainly germinates at lower nodes [6]. In this study, under both 15 and 40 cm stubble treatments, the single-bud length and the number of viable buds per unit area of LJY1212 were highest at the uppermost node and decreased gradually as node position moved downward (Figs. 2 and 3), which may be because early-germinating dominant buds inhibit further growth of buds at other nodes through hormone and nutrient competition [26]. In addition, under the 40 cm stubble treatment, the differences in single-bud length and number of viable buds per unit area between the uppermost node and the other nodes of LJY1212 were greater than those under the 15 cm stubble treatment, indicating that the higher the stubble height, the stronger the axillary bud germination dominance [15].

Unlike LJY1212, YY4949 exhibited the highest single-bud length and number of viable buds per unit area at the sub-upper node under both 15 and 40 cm stubble treatments (Figs. 2 and 3). In addition, the I2 internode of LJY1212 was longer than that of YY4949, whereas the I3 internode was shorter than that of YY4949, and the differences in I4 and I5 internode lengths were small (Fig. S6); therefore, the I2 internode retained by YY4949 under the 40 cm stubble treatment was shorter. Increases in stubble dry matter weight and non-structural carbohydrate content are beneficial for improving ratoon bud germination and increasing ratoon-season yield [32,33]. Although YY4949 retained a longer I3 internode under the 15 cm stubble treatment, ratoon bud germination in low-node-position-dominant varieties is inherently slow, and reducing stubble height further delays ratoon bud germination [12,34]. On the other hand, low stubble promotes the formation of ratoon roots from lower-position ratoon tillers, thereby enhancing the plant's ability to directly absorb soil water and nutrients [31]. If upper-node ratoon buds grow and develop rapidly, they can form photosynthetic leaves earlier, provide assimilates for ratoon tiller growth, and may help maintain the physiological activity of the stubble [18]. However, under the 15 cm stubble treatment, the upper-node ratoon buds of YY4949 grew slowly and lacked ratoon roots (Figs. S4 and S5), causing the stubble internodes to gradually lose physiological activity or even die, resulting in a higher mortality rate of ratoon buds at these nodes.

This study also found that LJY1212 exhibited a "fewer but longer roots" pattern, whereas YY4949 exhibited a "more numerous and thicker roots" pattern. In addition, under the 40 cm stubble treatment, root growth of LJY1212 appeared to be better than under the 15 cm stubble treatment, whereas YY4949 showed the opposite response trend (Figs. S4 and S5). Thick roots are mainly responsible for water and nutrient transport, whereas fine roots are mainly responsible for water and

nutrient uptake [35]. Previous studies have shown that higher root vitality and stronger root regeneration capacity are conducive to maintaining water and nutrient supply in ratoon rice and are closely associated with higher ratoon-season yield [14]. Therefore, the "more numerous and thicker roots" root system formed by YY4949 may possess greater root biomass and stronger water and nutrient transport capacity, which is beneficial for maintaining material supply and growth vigor of ratoon plants, thereby providing a better root foundation for rapid ratoon bud growth and subsequent yield formation.

4.3 Integrated metabolomic and transcriptomic analysis

In this study, integrated metabolomic and transcriptomic analyses systematically revealed the metabolic and transcriptional regulatory characteristics of rice varieties with different node-position dominance types during ratoon bud germination. PCA showed that germinated and non-germinated ratoon buds of LJY1212 and YY4949 were clearly separated, whereas germinated and non-germinated ratoon buds of the same variety under different stubble heights clustered together, indicating that stubble height itself does not alter the overall regulatory pattern of ratoon bud germination (Fig. 4A and Fig. 5A). Transcriptomic and metabolomic analyses indicated that the two varieties underwent relatively consistent metabolic and transcriptional reprogramming during ratoon bud germination. Both omics layers were jointly enriched in functional modules such as carbon metabolism, antioxidant metabolism, and secondary metabolism, and these processes may coordinate cell division, elongation, and material and energy supply during ratoon bud germination (Fig. 4D, Fig. 5E, and Table S1). Further comparison of the specific response differences between the two varieties showed that the DEGs specific to LJY1212 were mainly enriched in protein synthesis, photosynthetic energy supply, and fatty acid metabolism pathways (Fig. 4E), while its DAMs were mainly enriched in central carbon metabolism and photosynthetic carbon fixation pathways (Fig. 5D), suggesting that LJY1212 may enhance carbon source acquisition and utilization efficiency, strengthen the supply of ATP and metabolic intermediates, and simultaneously enhance protein synthesis and photosynthetic structure construction, thereby providing sufficient material and energy basis for rapid cell division, elongation, and tissue formation during ratooning. In contrast, the DEGs specific to YY4949 were mainly involved in the regulation of sulfur-containing amino acid metabolism, sugar metabolism, lipid metabolism, and antioxidant defense (Fig. 4E), while its DAMs were mainly enriched in antioxidant defense, redox homeostasis, and sugar-lipid metabolic regulation (Fig. 5D), suggesting that YY4949 may reduce cellular damage caused by excess reactive oxygen species and ensure the stable operation of membrane systems and basal metabolic processes by strengthening the antioxidant system, regulating sugar-lipid metabolism, and maintaining a suitable redox environment, thereby maintaining the physiological activity and sustained differentiation capacity of ratoon cells.

Integrated metabolomic and transcriptomic analyses highlighted that zeatin biosynthesis, starch and sucrose metabolism, and ascorbate and aldarate metabolism pathways all responded to varying degrees. Hormones such as IAA, CTK, and SL play core roles in regulating apical dominance

release and lateral bud germination, with IAA mainly maintaining bud dormancy and CTK promoting bud activation and cell division [20,36]. CTKs are adenine derivatives that mainly occur as isoprenoid forms, including trans-zeatin (tZ), cis-zeatin (cZ), dihydrozeatin (DZ), and isopentenyladenine (iP), among which tZ-type and iP-type cytokinins are the main functional forms in plants [37]. In this study, ZR content increased during ratoon bud germination (Fig. 7), whereas the expression of IPT genes decreased, and the expression of UGT73C and cisZOG genes also decreased (Fig. 6a and Fig. S7), indicating that a relatively high level of active cytokinins may be maintained during ratoon bud germination by reducing cytokinin inactivation. Previous studies have shown that IAA can reduce CTK levels by inhibiting IPT expression, thereby maintaining bud dormancy, whereas overexpression of OsIPT genes can increase CTK accumulation and promote axillary bud formation in rice [38,39]. cisZOGT can catalyze the O-glucosylation of oT, and more rapid O-glucosylation may lead to lower accumulation of cZRPs [40,41]. Therefore, these results suggest that the maintenance of CTK levels during ratoon bud germination may not mainly depend on enhanced local de novo synthesis, but is more closely related to reduced cytokinin inactivation and the regulation of metabolic homeostasis.

Starch and sucrose metabolism is an important basis for carbon source supply and energy utilization during ratoon bud germination, and sucrose can also act as a signaling molecule involved in the regulation of bud growth [42,43,44]. In this study, the sucrose content and sucrose synthase (SS) activity in germinated stem nodes were significantly higher than those in non-germinated stem nodes (Fig. 7), indicating that increased sucrose content is beneficial for ratoon bud germination and growth [7]. Transcriptomic analysis showed that SUS, INV, and HK genes related to sucrose metabolism each included both upregulated and downregulated members (Fig. 6b), suggesting that sucrose decomposition and hexose utilization are differentially regulated. Meanwhile, AMY- and otsB-related genes were upregulated (Fig. 6b). Nutrients in the stem sheath are stored in the form of starch and hydrolyzed to sucrose by α-amylase and β-amylase, providing a material basis for early ratoon bud germination and growth [15]. In addition, GN1_2_3, GN5_6, and bglB and bglX-related genes were upregulated (Fig. 7b), suggesting that amino sugar metabolism and β-glucoside hydrolysis may participate in carbohydrate turnover [45]. Comparison between varieties showed that PYG was predominantly upregulated in LJY1212, whereas pgm, SPS, and TPS were predominantly upregulated in YY4949 (Fig. 6b), suggesting that the former may focus more on metabolic regulation related to starch phosphorolysis, whereas the latter may focus more on sugar phosphate conversion, sucrose synthesis, and trehalose-related metabolic regulation. Meanwhile, WAXY was predominantly downregulated and ISA predominantly upregulated in both varieties (Fig. 6b). These results indicate that the carbon metabolic pathways of the two varieties share both commonalities and differences during ratoon bud germination. Metabolomic results showed that the metabolite trehalose accumulated significantly (Fig. 6b). Although trehalose cannot directly promote ratoon bud germination in rice, trehalose-6-phosphate (T6P), as its direct biosynthetic precursor, participates in axillary bud dormancy release and growth regulation [46,47]. Starch and

sucrose metabolism not only provides carbon sources and energy for ratoon bud germination but also enhances plant adaptability to abiotic stress by regulating soluble sugar accumulation, maintaining osmotic balance, and participating in reactive oxygen species (ROS) scavenging and antioxidant defense [48-50].

Ratoon bud germination and growth are accompanied by redox regulation. Mechanical damage caused by main crop harvest induces reactive oxygen species (ROS) accumulation, and ascorbate, as an important non-enzymatic antioxidant in plants, plays a key role in scavenging ROS and regulating cellular redox status [51]. In this study, the expression of AKR1A1 and GULO-related genes in the ascorbate and aldarate metabolism pathway was upregulated (Fig. 6c), suggesting that L-gulose- and aldarate-related metabolic processes may be altered. Previous studies have shown that some GULO homolog proteins may participate in ascorbate biosynthesis in plants [52]. In addition, VTC5 and VTC4 were upregulated; these two genes are involved in the conversion of GDP-L-galactose to L-galactose-1-phosphate and the conversion of the latter to L-galactose, respectively (Fig. 6c), suggesting that steps related to ascorbate biosynthesis may be regulated. Studies have shown that increasing the expression of GDP-L-galactose phosphorylase (GGP, also known as VTC2/VTC5) can increase ascorbate content in specific tissues and developmental stages [53]. Meanwhile, the upregulation of DHAR indicates that processes related to the reduction and regeneration of dehydroascorbate may be regulated (Fig. 7c); this enzyme participates in the conversion of DHA to ascorbate via glutathione [54]. Metabolomic results showed that the metabolites L-gulose and L-threonate were upregulated, whereas the metabolite 2-oxoglutarate was downregulated, further indicating that related sugar acid metabolism and ascorbate turnover processes may be altered (Fig. 6c). In addition, ALDH family genes showed both upregulation and downregulation in both varieties (Fig. 6c), indicating that their regulation differs. Given that some ALDH members participate in tryptophan-dependent IAA synthesis [55], there may be a link between ascorbate metabolism and hormone regulation, jointly affecting ratoon bud development.

5. Conclusions

Samples clustered primarily by genotype rather than by stubble height, indicating that although stubble height affects the germination dominance and resource allocation of ratoon buds, it does not alter the fundamental regulatory pattern of ratoon bud germination. In the high-node-position-dominant variety represented by LJY1212, plant hormone levels changed after apical dominance removal; ratoon buds at dominant nodes grew rapidly, relying mainly on nutrients supplied by the stubble, and further promoted growth through the gradual establishment of their own photosynthetic capacity. In contrast, in the low-node-position-dominant variety represented by YY4949, ratoon bud emergence was relatively slow; after apical dominance removal, processes related to antioxidant defense and secondary metabolism changed, accompanied by adjustments in plant hormone levels and the formation of ratoon roots, enabling ratoon buds to directly absorb water and nutrients from the soil through newly formed roots and providing material support for subsequent growth. Although the two varieties exhibited different node-position germination dominance and metabolic

regulatory characteristics, ratoon bud germination in both involved common processes such as plant hormone regulation, carbon and nitrogen metabolism, and antioxidant defense, indicating that the two varieties share a similar basal regulatory network, while differing in the magnitude of pathway responses, regulatory emphasis, and resource acquisition strategies, thereby forming distinct ratoon bud germination and growth strategies. This study reveals the relationship between shared regulatory mechanisms and variety-specific responses during ratoon bud germination in rice varieties with different node-position dominance types, providing a new perspective for understanding the differential regulatory mechanisms of ratoon bud germination and subsequent growth in rice (Fig. 8).

Authors contributions D.Y., and Q.T. conceptualized the study and supervised the research. P.G. conducted experiments, analyzed data, and drafted the manuscript. P.G., and Y.L. analyzed and interpreted the data and drafted the manuscript. P.G., L.Z., and J.H. conducted experiments.P.G., and Y.L. conducted experiments and analyzed data. P.G., D.Y., and Q.T. drafted the manuscript, and all authors reviewed and approved the final version.

Funding The study was supported by the Yuelushan Laboratory Talent Program (2024RC2038) and the National Key Research and Development Program of China (2022YFD2301000) .

Data availability Data will be available upon request

Declarations

Ethics approval and consent to participate Not applicable.

Consent for publication Not applicable.

Competing interests The authors declare no competing interests.

References:

1. Yuan S, Stuart AM, Laborte AG, Rattalino Edreira JI, Dobermann A, Le VNK, et al. Sout heast asia must narrow down the yield gap to continue to be a major rice bowl. Nat Food. 2022;3:217-26. doi:10.1038/S43016-022-00477-Z.
2. Lobell DB, Cassman KG, Field CB. Crop yield gaps: their importance, magnitudes, and ca uses. Annu Rev Environ Resour. 2009;34:179-204. doi: 10.1146/annurev.environ.041008.093740.
3. Peng SB. Reflection on china's rice production strategies during the transition period. Scient ia Sinica(Vitae). 2014;44:845-50. doi: 10.1360/052014-98.
4. Ray DK, Foley JA. Increasing global crop harvest frequency: recent trends and future directions. Environ Res Lett. 2013;8:44041-50. doi: 10.1088/1748-9326/8/4/044041.
5. Zheng C, Wang YC, Yuan S, Yu X, Yang GD, Yang C, et al. Effects of skip-row planting on grain yield and quality of mechanized ratoon rice. Nutr Metab (Lond). 2022;285:108584. doi: 10.1016/j.fcr.2022.108584.
6. Wang WQ, He AB, Jiang GL, Sun HJ, Jiang M, Man JG, et al. Ratoon rice technology: a green and resource-efficient way for rice production. Adv Agron. 2020;159:135-67. doi: 10.3390/agronomy12112837.
7. He AB, Min J, Nie LX, Man JG, Peng SB. Effects of source-sink regulation and nodal position of the main crop on the sprouting of regenerated buds and grain yield of ratoon rice. Innov Food Sci Emerg Technol. 2023;14:1043354. doi: 10.3389/fpls.2023.1043354.
8. Xi M, Xu YZ, Li Z, Hu R, Cheng TP, Zhou YJ, et al. Progress and challenges of rice ratooning technology in anhui province, china. Crop and Environment. 2023;2:81-6. doi:

10.1016/j.crope.2023.04.003.
9. Yu X, Guo Y, Yang GD, Zhang ZL, Liang YJ, Zheng C, et al. Nitrogen response of regenerated tillers varied among node positions in ratoon rice. Field Crops Res. 2022;289:108717. doi: 10.1016/J.FCR.2022.108717.
10. Nakano H, Takai T, Kondo M. Identification of quantitative trait loci for panicle structure and grain filling using a cross between indica- and japonica- type high-yielding rice cultivars. Plant Prod Sci. 2019;22:443-55. doi: 10.1080/1343943X.2019.1667836.
11. Yi ZX, Wang XH, Chen PP, Zhou WX, Tui NM. Differences in ratooning characteristics of axillary buds of hybrid rice with different ratooning types between in vivo and in vitro. Hybrid Rice. 2008;23:73-6. doi: 10.16267/j.cnki.1005-3956.2008.05.025.
12. Harrell DL, Bond JA, Blanche S. Evaluation of main-crop stubble height on ratoon rice growth and development. Field Crops Res. 2009;114:396-403. doi: 10.1016/j.fcr.2009.09.011.
13. Nakano H, Tanaka R, Nakagomi K, Hakata M. Grain yield response to stubble leaf blade clipping in rice ratooning in southwestern japan. Agron J. 2021;113:4013-21. doi: 10.1002/AGJ2.20834.
14. Xu FX, Zhang L, Zhou XB, Guo XY, Zhu YC, Liu M, et al. The ratoon rice system with high yield and high efficiency in china: progress, trend of theory and technology. Field Crops Res. 2021;272:108282. doi: 10.1016/j.fcr.2021.108282.
15. Wu YJ, Li Y, Wang BF, Zhang ZS, Xie Y, Zhang ZL, et al. Research progress on the influencing factors of regenerated bud germination and growth in ratoon rice. China Rice. 2025;31:39-46. doi: 10.3969/j.issn.1006-8082.2025.05.006.
16. Lin WF, Guo CL, Lan CJ, Xie YB, Qin B, Zhan GM, et al. Research progress and cultivation strategies for ratoon rice under mechanical harvesting conditions. Journal of Zhejiang University (Agric. & Life Sci.). 2025;51:350-65. doi: 10.3785/j.issn.1008-9209.2023.12.122.
17. Lin WX, Weng PY, Lin WF, Shao CH, Guo CL, Li Z, et al. Research status and prospect of ratoon rice in china under mechanically harvested condition. Chinese Journal of Applied Ecology. 2024;35:827-36. doi: 10.13287/j.1001-9332.202403.008.
18. Yi ZX, Tu NM, Wang P, Chen PP. Ratooning properties of axillary buds of two-line hybrid rice in vivo and in vitro. Acta Agronomica Sinica. 2005;31:330-6. doi: 10.3321/j.issn:0496-3490.2005.03.010.
19. Amelie R, Clemence H, Khaoula BB, Eric M, Wassim A, Jeremy L, et al. Insight into the role of sugars in bud burst under light in the rose. Plant Cell Physiol. 2012;53:1068-82. doi: 10.1093/pcp/pcs051.
20. Barbier FF, Dun EA, Kerr SC, Chabikwa TG, Beveridge CA. An update on the signals controlling shoot branching. Trends Plant Sci. 2019;24:220-36. doi: 10.1016/j.tplants.2018.12.001.
21. Sunita K, Ashverya L. The interaction between glucose and cytokinin signal transduction pathway in arabidopsis thaliana. Plant Cell Environ. 2014;37:235-53. doi: 10.1111/pce.12149.
22. Tessi TM, Brumm S, Winklbauer E, Schumacher B, Pettinari G, Lescano I, et al. Arabidopsis AZG2 transports cytokinins in vivo and regulates lateral root emergence. New Phytol. 2021;229:979-93. doi: 10.1111/nph.16943.
23. Jiang L, Liu X, Xiong GS, Liu HH, Chen FL, Wang L, et al. DWARF 53 acts as a repressor of strigolactone signalling in rice. Nature. 2013;504:401-5. doi: 10.1038/nature12870.
24. Brewer PB, Dun EA, Gui RY, Mason M, Beveridge CA. Strigolactone inhibition of branching independent of polar auxin transport. Plant Physiol. 2015;168:1820-32. doi: 10.1104/pp.15.00014.
25. González-Grandío E, Pajoro A, Franco-Zorrilla JM, Tarancón C, Cubas P. Abscisic acid signaling

is controlled by a BRANCHED1/HD-ZIP i cascade in arabidopsis axillary buds. Proc Natl Acad Sci U S A. 2016;114:E245. doi: 10.1073/pnas.1613199114.
26. Dun EA, Alexandre GSD, Rameau C, Beveridge CA. Antagonistic action of strigolactone and cytokinin in bud outgrowth control. Plant Physiol. 2012;158:487-98. doi: 10.1104/pp.111.186783.
27. Bennett T, Sieberer T, Willett B, Booker J, Luschnig C, Leyser O. The arabidopsis MAX pathway controls shoot branching by regulating auxin transport. Curr Biol. 2006;16:553-63. doi: 10.1016/j.cub.2006.01.058.
28. Ku WZ, Su Y, Peng XY, Wang RZ, Li HO, Xiao LT. Comparative transcriptome analysis reveals inhibitory roles of strigolactone in axillary bud outgrowth in ratoon rice. Plants (Basel). 2024;13:899-914. doi: 10.3390/plants13060899.
29. Zhang Q, Liu XC, Yu GL, Wang H, Feng DQ, Zhao HY, et al. Agronomic and physiological characteristics of high-yielding ratoon rice varieties. Agron J. 2021;113:5063-75. doi: 10.1002/agj2.20871.
30. Hoff BJ, Bollich PK. Node origin of ratoon tillers of u.s. Rice varieties. Report of Projects, Department of Agronomy. 1989:84-7.
31. Lin WX, Chen HF, Zhang ZX, Xu QH, Tu NM, Fang CX, et al. Research and prospect on physio-ecological properties of ratoon rice yield formation and its key cultivation technology. Chinese Journal of Eco-Agriculture. 2015;23:392-401. doi: 10.13930/j.cnki.cjea.150246.
32. He AB, Wang WQ, Jiang GL, Sun HJ, Jiang M, Man JG, et al. Source-sink regulation and its effects on the regeneration ability of ratoon rice. Field Crops Res. 2019;236:155-64. doi: 10.1016/j.fcr.2019.04.001.
33. Yazdpour H, Shahri MM, Soleymani A, Shahrajabian MH. Effects of harvesting time and harvesting height on grain yield and agronomical characters in rice ratoon (oryza sativa l.). Journal of Food Agriculture and Environment. 2012;10:438-40.
34. Chen JQ, Liu ZB, Li YZ, Wang L, Gao C, Jiang JH. Study on stubble height in perennial japonica rice. Fujian Science and Technology of Rice and Wheat. 1996;16:22-4. doi: CNKI:SUN:FJDM.0.1996-04-005.
35. Blouin, M., Barot, S., Roumet, C., 2007. A quick method to determine root biomass distribution in diameter classes. Plant Soil 290, 371-381. https://doi.org/10.1007/s11104-006-9169-1
36. Kotov AA, Kotova LM, Romanov GA. Signaling network regulating plant branching: recent advances and new challenges. Plant Sci. 2021;307:110880-91. doi: 10.1016/J.Plantsci.2021.110880.
37. Werner T, Schmülling T. Cytokinin action in plant development. Curr Opin Plant Biol. 2009;12:527-38. doi: 10.1016/j.pbi.2009.07.002.
38. Sakakibara H. Cytokinins: activity, biosynthesis, and translocation. Annu Rev Plant Biol. 2006;57:431-49. doi: 10.1146/annurev.arplant.57.032905.105231.
39. Ferguson BJ, Beveridge CA. Roles for auxin, cytokinin, and strigolactone in regulating shoot branching. Plant Physiol. 2009;149:1929-44. doi: 10.1104/pp.109.135475.
40. Kudo T, Makita N, Kojima M, Tokunaga H, Sakakibara H. Cytokinin activity of cis-zeatin and phenotypic alterations induced by overexpression of putative cis-zeatin-o-glucosyltransferase in rice1[c][w][OA]. Plant Physiol. 2012;160:319-31. doi: 10.1104/pp.112.196733.
41. Mok MC, Martin RC, Dobrev PI, Vanková R, Shing Ho P, Yonekura-Sakakibara K, et al. Topolins and hydroxylated thidiazuron derivatives are substrates of cytokinin o-glucosyltransferase with position specificity related to receptor recognition. Plant Physiol. 2005;137:1057-66. doi: 10.1104/pp.104.057174.

42. MacNeill GJ, Mehrpouyan S, Minow MAA, Patterson JA, Tetlow IJ, Emes MJ. Starch as a source, starch as a sink: the bifunctional role of starch in carbon allocation. J Exp Bot. 2017;68:4433-53. doi: 10.1093/jxb/erx291.
43. Mason MG, Ross JJ, Babst BA, Wienclaw BN, Beveridge CA. Sugar demand, not auxin, is the initial regulator of apical dominance. Proc Natl Acad Sci U S A. 2014;111:6092-7. doi: 10.1073/pnas.1322045111.
44. Schneider A, Godin C, Boudon F, Demotes-Mainard S, Sakr S, Bertheloot J. Light regulation of axillary bud outgrowth along plant axes: an overview of the roles of sugars and hormones. Front Plant Sci. 2019;10:1296. doi: 10.3389/fpls.2019.01296.
45. Ketudat Cairns JR, Mahong B, Baiya S, Jeon JS, Jeon JS. β-glucosidases: multitasking, moonlighting or simply misunderstood? Plant Sci. 2015;241:246-59. doi: 10.1016/j.plantsci.2015.10.014.
46. Fichtner F, Fichtner F, Barbier FF, Annunziata MG, Feil R, Olas JJ, et al. Regulation of shoot branching in arabidopsis by trehalose 6-phosphate. The New Phytologist. 2021;229:2135-51. doi: 10.1111/nph.17006.
47. Kerbler SM, Armijos-Jaramillo V, Lunn JE, Vicente R. The trehalose 6-phosphate phosphatase family in plants. Physiol Plant. 2023;175:e14096. doi: 10.1111/ppl.14096.
48. Dong SY, Beckles DM. Dynamic changes in the starch-sugar interconversion within plant source and sink tissues promote a better abiotic stress response. J Plant Physiol. 2019;234-235:80-93. doi: 10.1016/j.jplph.2019.01.007.
49. Lemoine R, La Camera S, Atanassova R, Dédaldéchamp F, Allario T, Pourtau N, et al. Source-to-sink transport of sugar and regulation by environmental factors. Front Plant Sci. 2013;4:272-92. doi: 10.3389/fpls.2013.00272.
50. Morris SE, Cox MCH, Ross JJ, Krisantini S, Beveridge CA. Auxin dynamics after decapitation are not correlated with the initial growth of axillary buds. Plant Physiol. 2005;138:1665-72. doi: 10.1104/pp.104.058743.
51. Wu PW, Li BW, Liu Y, Bian Z, Xiong JX, Wang YX, et al. Multiple physiological and biochemical functions of ascorbic acid in plant growth, development, and abiotic stress response. International journal of molecular sciences. 2024;25:1832-48. doi: 10.3390/ijms25031832.
52. Maruta T, Ichikawa Y, Mieda T, Takeda T, Tamoi M, Yabuta Y, et al. The contribution of arabidopsis homologs of l-gulono-1,4-lactone oxidase to the biosynthesis of ascorbic acid. Biosci Biotechnol Biochem. 2010;74:1494-7. doi: 10.1271/bbb.100157.
53. Broad RC, Bonneau JP, Beasley JT, Roden S, Sadowski P, Jewell N, et al. Effect of rice GDP-l-galactose phosphorylase constitutive overexpression on ascorbate concentration, stress tolerance, and iron bioavailability in rice. Front Plant Sci. 2020;11:595439. doi: 10.3389/fpls.2020.595439.
54. Smirnoff N, Wheeler GL. The ascorbate biosynthesis pathway in plants is known but there is a way to go with understanding control and functions. J Exp Bot. 2024;75:2604-30. doi: 10.1093/JXB/ERAD505.
55. Wang JJ, Wang RX, Liu L, Zhang WR, Yin ZH, Guo R, et al. Integrated physiological, transcriptomic and metabolomic analyses of the response of rice to aniline toxicity. International Journal of Molecular Sciences. 2025;26:582-606. doi: 10.3390/ijms26020582.

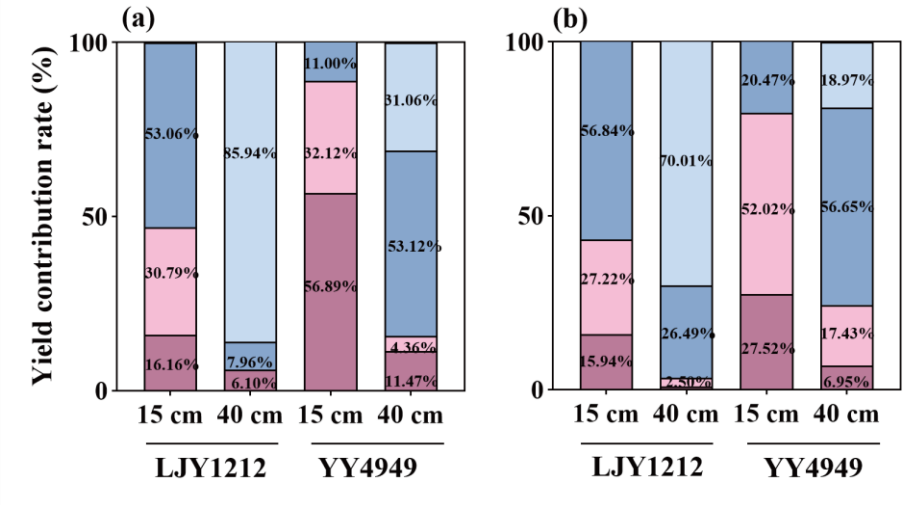


Fig. 1 Yield contribution rates of ratoon tillers at the second, third, fourth, and fifth uppermost nodes (D2, D3, D4, and D5) of the two varieties under different stubble heights in the 2024 and 2025 ratoon seasons. 15 cm, 15 cm stubble height; 40 cm, 40 cm stubble height. LJY1212, Longjingyou 1212; YY4949, Yongyou 4949.

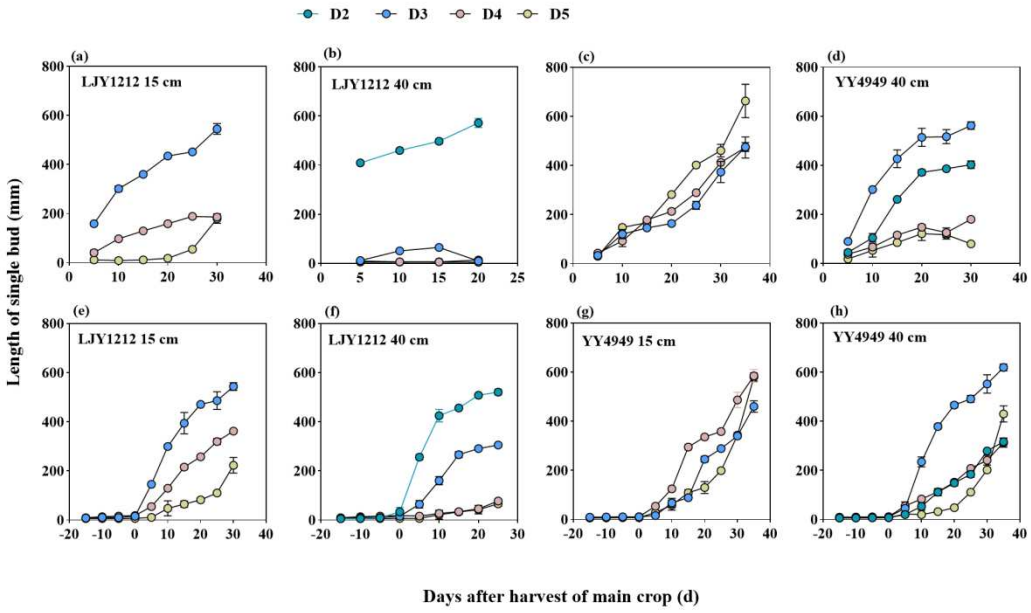


Fig. 2 Dynamic changes in ratoon tiller length at the second, third, fourth, and fifth uppermost nodes (D2, D3, D4, and D5) of the two varieties under different stubble heights in 2024 (a, b, c, d) and 2025 (e, f, g, h). 15 cm, 15 cm stubble height; 40 cm, 40 cm stubble height. LJY1212, Longjingyou 1212; YY4949, Yongyou 4949.

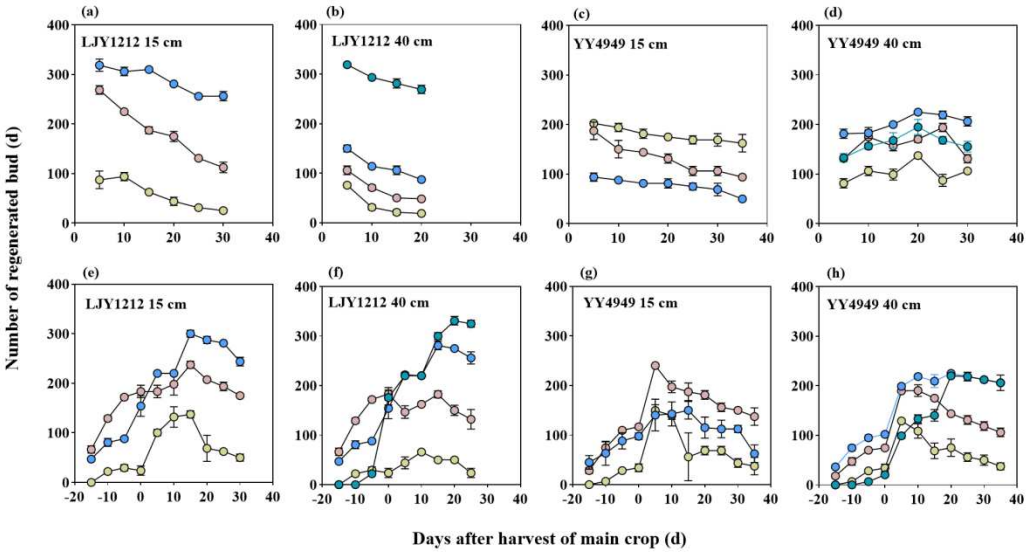


Fig. 3 Dynamic changes in the number of viable ratoon tillers at the second, third, fourt, and fifth uppermost nodes (D2, D3, D4, and D5) of the two varieties under different stubble heights in 2024 (a, b, c, d) and 2025 (e, f, g, h). 15 cm, 15 cm stubble height; 40 cm, 40 cm stubble height. LJY1212, Longjingyou 1212; YY4949, Yongyou 4949.

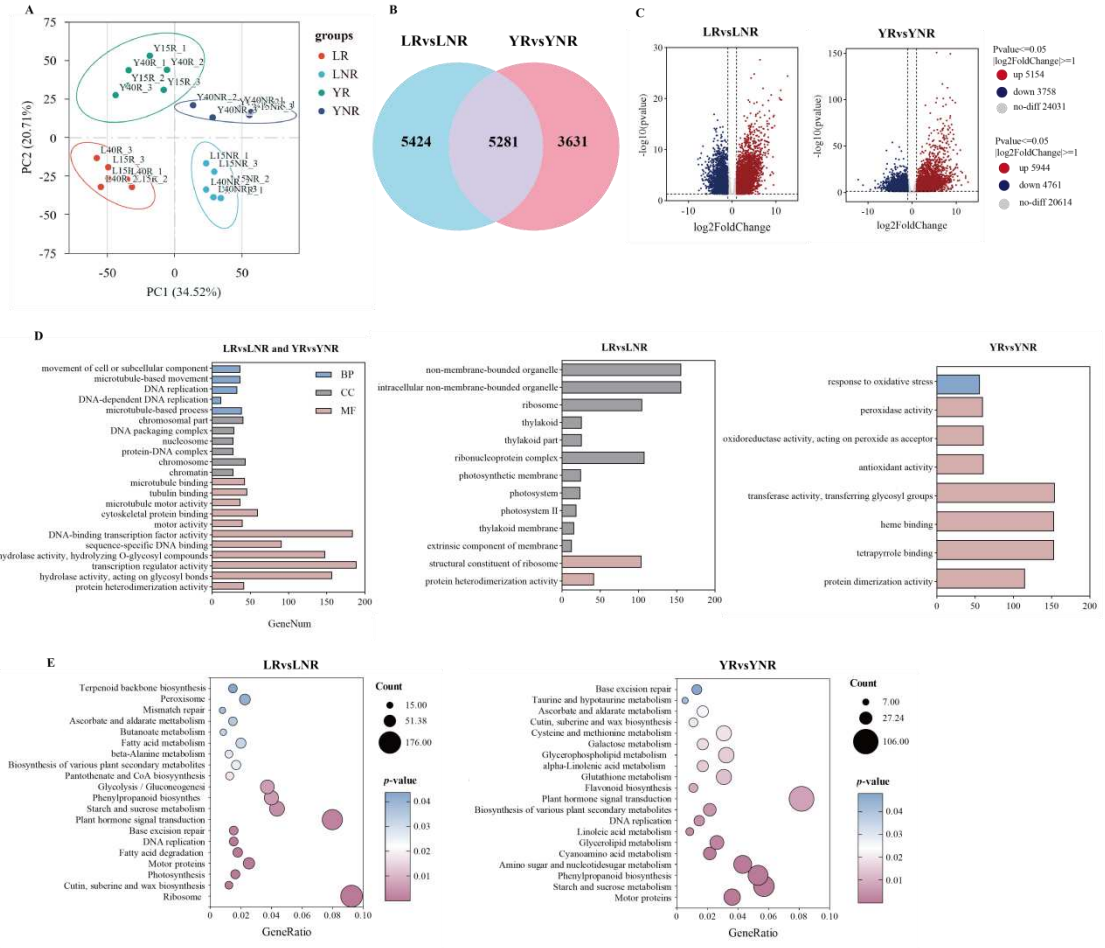


Fig. 4 Transcriptomic changes during ratoon bud germination in rice varieties with different node-position dominance types. (A) Principal component analysis (PCA); (B) Venn diagram analysis of DEGs; (C) Bubble plot of DEGs; (D) GO functional enrichment analysis; (E) KEGG pathway enrichment analysis.

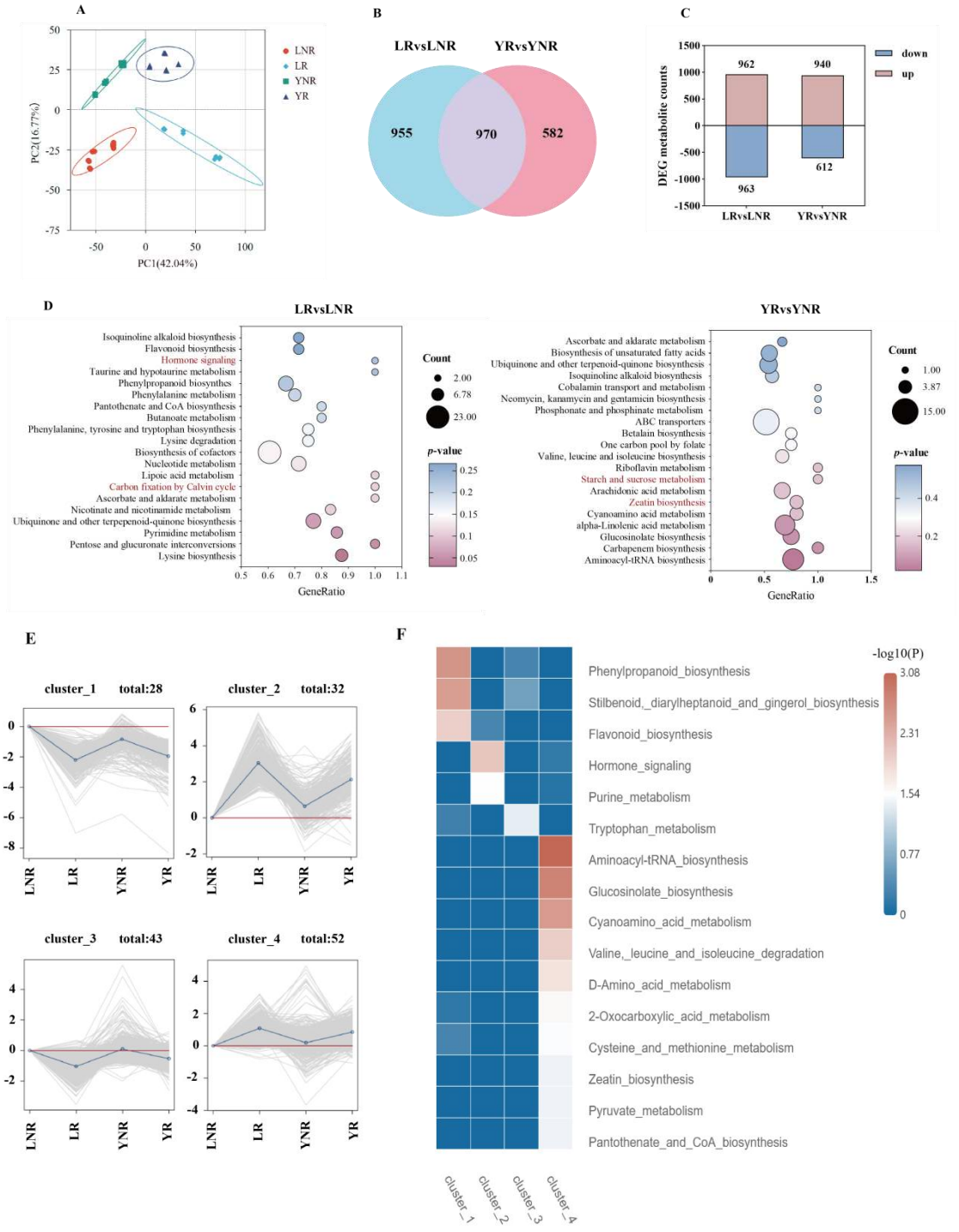


Fig. 5 Metabolomic changes during ratoon bud germination in rice varieties with different node-position dominance types. (A) Principal component analysis (PCA); (B) Venn diagram analysis of DAMs; (C) Bar chart of DAMs; (D) Bubble plot of KEGG enrichment; (E) K-means clustering analysis; (F) KEGG enrichment analysis of differentially accumulated metabolites.

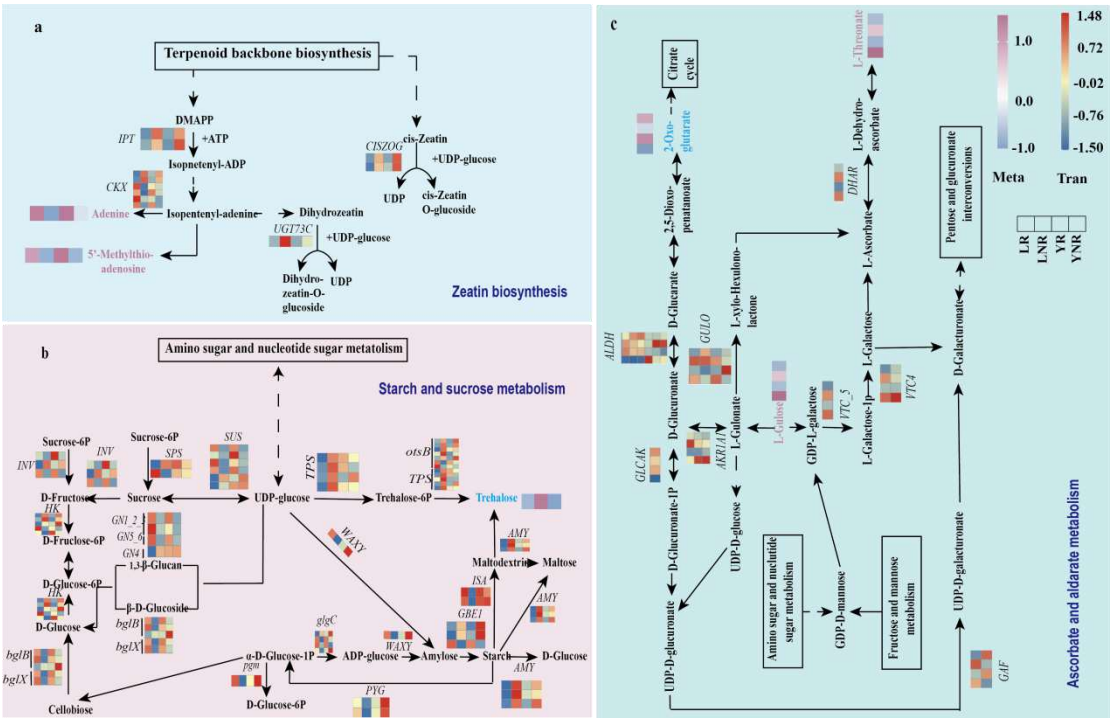


Fig. 6 Differences in gene expression and metabolite content in metabolic pathways related to zeatin biosynthesis, starch and sucrose metabolism, and ascorbate and aldarate metabolism during ratoon bud germination in the two varieties. (a) Zeatin biosynthesis-related pathway; (b) starch and sucrose metabolism-related pathway; (c) ascorbate and aldarate metabolism-related pathway. In the heatmaps, each row represents a gene or metabolite, and each column represents the germinated and non-germinated ratoon bud samples of LJY1212 and YY4949 in sequence. Orange-red and blue heatmaps indicate gene expression abundance, while pink and light blue heatmaps indicate the relative abundance of metabolites. Enzyme annotations: IPT, isopentenyltransferase; CKX, cytokinin oxidase; CISZOG, glucosyltransferase; UGT73C, UDP-glycosyltransferase; INV, invertase; HK, hexokinase; bglB, β-glucosidase; bglX, β-glucosidase; SPS, sucrose phosphate synthase; GN1_2_3, glucosamine-6-phosphate isomerase 1/2/3; GN5_6, glucosamine-6-phosphate N-acetyltransferase 5/6; GN4, glucosamine-6-phosphate N-acetyltransferase 4; N-acetylglucosaminidase; TPS, trehalose-6-phosphate synthase; WAXY, granule-bound starch synthase; pgm, phosphoglucomutase; glgC, glucose-1-phosphate adenylyltransferase; PYG, glycogen phosphorylase; otsB, trehalose-6-phosphate phosphatase; AMY, α-amylase; ISA, starch debranching enzyme; GBE1, 1,4-α-glucan branching enzyme; GLCAK, glucuronokinase; ALDH, aldehyde dehydrogenase; AKR1A1, aldo-keto reductase; GULO, L-gulono-1,4-lactone oxidase; VTC2_5, GDP-L-galactose phosphorylase; VTC4, L-galactose-1-phosphate phosphatase; DHAR, dehydroascorbate reductase; GAE, UDP-glucuronate 4-epimerase.

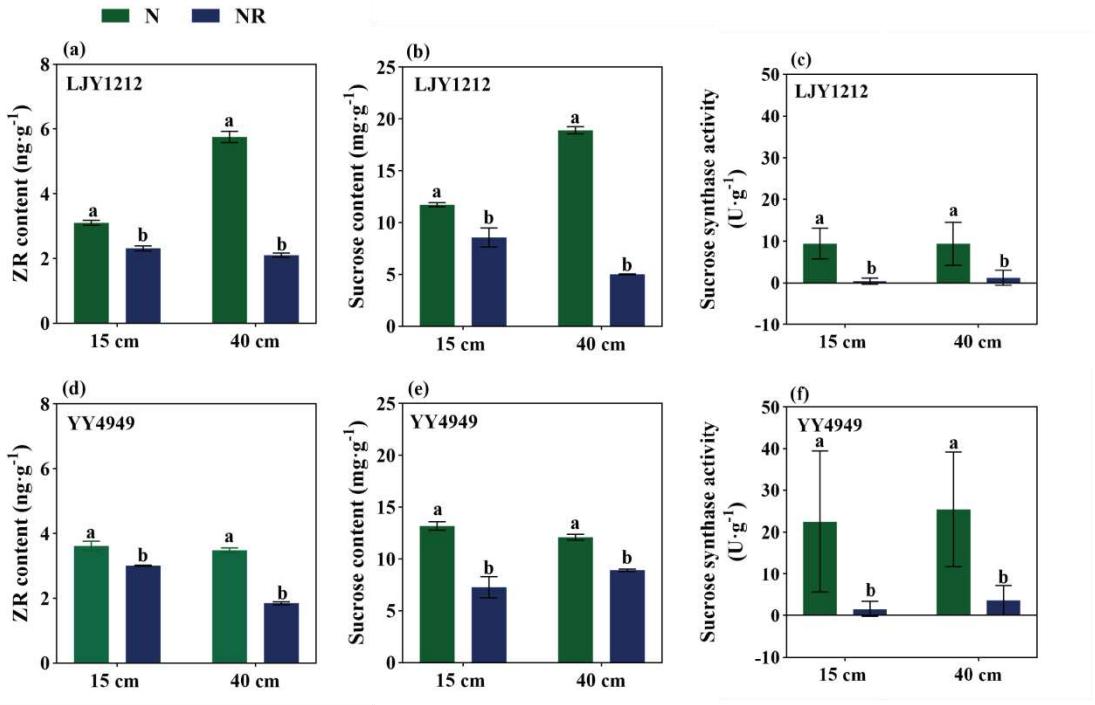


Fig. 7. Changes in zeatin riboside content, sucrose content, and sucrose synthase activity in sprouted and non-sprouted nodal tissues of LJY1212 and YY4949. N: germinated ratoon stem buds; NR: non-germinated ratoon stem buds.

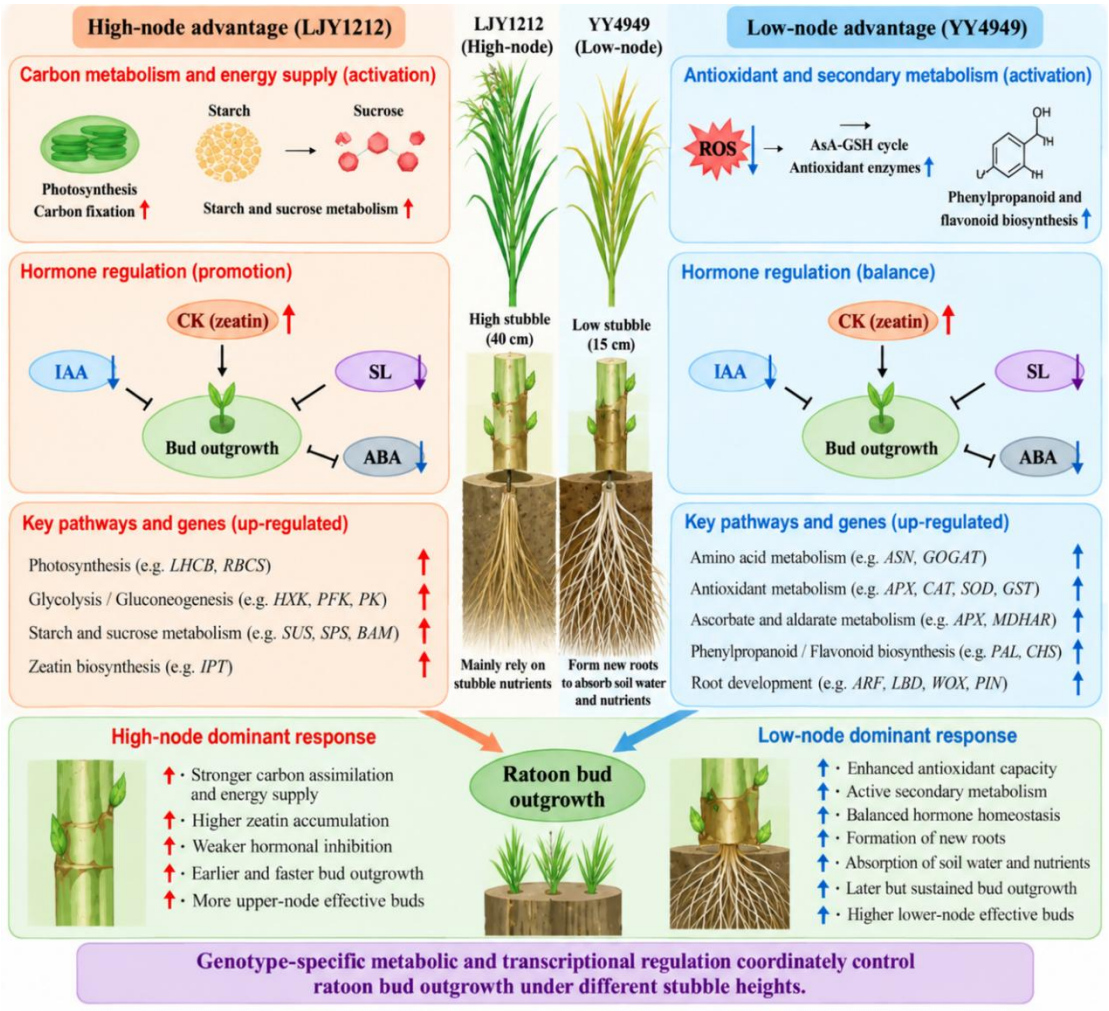


Fig. 8 Differences in the mechanisms of ratoon bud germination among rice varieties with different node-position ratooning types

Supplementary Files

This is a list of supplementary files associated with this preprint. Click to download.

- 2026.10.20SupplementaryFigure.docx
- SupplementaryTable.xlsx